Three-dimensional optical vortex and necklace solitons in highly nonlocal nonlinear media

Wei-Ping Zhong[1] and Milivoj Belić[2]
[1]*Department of Electronic Engineering, Shunde College, Guangdong Province, Shunde 528300, China*
[2]*Texas A & M University at Qatar, 23874 Doha, Qatar*
(Received 21 September 2008; published 2 February 2009)

We demonstrate the existence of localized optical vortex and necklace solitons in three-dimensional (3D) highly nonlocal nonlinear media, both analytically and numerically. The 3D solitons are constructed with the help of Kummer's functions in spherical coordinates and their unique properties are discussed. The procedure we follow offers ways for generation, control, and manipulation of spatial solitons.

DOI: 10.1103/PhysRevA.79.023804 PACS number(s): 42.65.Tg

I. INTRODUCTION

Spatial optical solitons are self-trapped beams of finite spatial cross section that travel without divergence associated with the freely diffracting beams. Owing to their novel physics, as well as potential applications, spatial solitons have been under intensive study in the past decade [1] and rich dynamics associated with them have been discovered. Vortex solitons are optical beams that have phase singularities mixed within the wave front curvature, and frequently appear in the study of optical tweezers [2], trapping and guiding of cold atoms [3], and entanglement states of photons [4]. Necklace solitons are a special class of self-trapped beams, which look like necklaces with the intensity and phase modulated periodically along the azimuthal angle [5]. Soljacic *et al.* predicted quasistable necklace beams in a Kerr nonlinear (NL) medium theoretically [6], and recently such beams were observed experimentally [7]. Necklace vector solitons also exhibit quasistable evolution in a saturable NL medium, although with a slowly expanding rate [8]. It was shown that the presence of topological charges can slow the expansion of such beams. Metastable necklace solitons were observed in lead glasses with a thermal nonlocal nonlinearity [9]. Robust spatiotemporal necklace solitons in the cubic-quintic Ginzburg-Landau system were reported in [10]. Dark hollow beams have also attracted attention, thanks to their potential for applications in the turbulent atmosphere [11]. However, almost all necklace solitons reported so far inevitably experience expansion during propagation, due to a net outward force exerted on each "pearl" by all other pearls forming the necklace [6].

Nonlocality has also been a phenomenon of intense research over recent years in various NL physical systems [1]. Basically, nonlocality extends the effect of localized excitations in a medium, allowing a degree of interconnection among different regions of the medium in question [12]. It has been shown recently that the stability of localized waves is greatly enhanced in nonlocal nonlinear (NN) media. In such media the NL response at a particular spatial location is determined by the wave intensity in the neighborhood of this location. Nonlocality often results from certain transport processes, such as atomic diffusion [13]. It can also be a signature of a long-range interparticle interaction, e.g., in nematic liquid crystals [14]. A spatially nonlocal (NLO) response is also naturally present in atomic condensates, where it describes a noncontact bosonic interaction [15]. Extensive studies of beam propagation in NN media revealed a range of interesting features. In particular, it has been shown that nonlocality may affect modulational instability of plane waves [16] and prevent catastrophic collapse of finite beams [17], as well as stabilize complex one-, two-, and three-dimensional beams, including vortices [18–20]. Recently, it has been shown that NLO media can support stable propagation of rotating solitons, the so-called azimuthons [21]. Recent theoretical studies demonstrated both stable and unstable evolution of azimuthons [22,23]. In the latter case it has been shown that in a highly NLO regime the azimuthons can undergo structural transformation resulting from the energetic coexistence of solitons of different symmetries. Numerical and analytical studies revealed that the angular velocity of azimuthons is governed by two contributions. There is the linear component, determined solely by the spatial structure of the beam (akin to the rotation of complex wave structures resulting from the beating of their constituent modes), as well as the NL component, which is brought about by the nonlinearity [22].

In this work, we investigate in detail three-dimensional (3D) highly NN solitons. We consider models for highly NN media where the spatial solitons have already been observed, such as lead glasses exhibiting self-focusing thermal nonlinearity [24], photorefractive media [25], and nematic liquid crystals [14]. We study NL waves in a generic, highly NLO optical system by solving the nonlocal nonlinear Schrödinger equation (NNSE), using the self-similar method. We demonstrate breathers whose evolution is periodic and discuss solitons in highly NN systems. We demonstrate that, by choosing a suitable soliton parameter, the solitons can be conveniently controlled and manipulated.

The paper is arranged as follows. In Sec. II we introduce the highly NN model and obtain the self-similar breather and soliton solutions in spherical coordinates. In Sec. III we compare our exact analytical results with the numerical solutions. One of our main findings, that the azimuthons emerge from the internal modes of stationary highly NN soliton solutions, like vortices and necklaces, is detailed in Sec. IV. Section V presents conclusions.

II. THE GENERAL NN MODEL AND SELF-SIMILAR SOLITON SOLUTIONS

A. Highly NN model

We consider an optical beam propagating along the z axis of a NL self-focusing material with the scalar amplitude of the electric field $E(\vec{r},t)=\Psi(\vec{r},t)\exp(i\vec{k}\cdot\vec{r}-i\varpi t)+\text{c.c.}$ Here $\vec{r}=(x,y,z)$, $\vec{k}$ is the wave number vector, ϖ is the optical frequency, and $\Psi(\vec{r},t)$ is the slowly varying amplitude. We assume that the refractive index change $N(I)$, induced by the beam intensity $I(\vec{r},t)=|\psi|^2$, can be described by the NLO model

$$N(I)(\vec{r},t)=\int R(\vec{r}-\vec{r}')I(\vec{r}',t)d\vec{r}'. \tag{1}$$

The response function $R(\vec{r})$ is assumed to be a real, positive definite, localized, and rotationally symmetric function [i.e., $R(\vec{r})=R(r)$] that satisfies the normalization condition $\int R(\vec{r})d\vec{r}=1$. The width of the response function $R(r)$ determines the degree of nonlocality. For a singular response $R(\vec{r})=\delta(\vec{r})$, the refractive index becomes a local function of the light intensity, $N(I)=I(\vec{r},t)$, i.e., the refractive index change at a given point is solely determined by the light intensity at that very point. With increasing width of $R(\vec{r})$ the light intensity in the vicinity of the point $\vec{r}$ also contributes to the index change at that point. In the opposite limit, when the response function is much broader than the intensity distribution, the NL term becomes proportional to the response function, $N(I)=-PR$, where P is the beam power. The NLO response (1) leads to the following NNSE governing the evolution of an optical beam in appropriately chosen dimensionless coordinates:

$$i\frac{\partial\psi}{\partial t}+\frac{1}{2}\nabla^2\psi+N(I)\psi=0. \tag{2}$$

It has been shown that as long as the response function is monotonically decaying, the physical properties of solutions to Eq. (2) do not depend strongly on its shape [16–20]. For convenience in our calculations we choose to work with the Gaussian response function

$$R(\vec{r}-\vec{r}')=\frac{1}{\pi\sigma^2}e^{-|\vec{r}-\vec{r}'|^2/\sigma^2}. \tag{3}$$

Assuming that the intensity distribution is peaked at the origin, one can expand the response function at the origin, to obtain $N(I)\approx-P(R_0+R_2r^2)$. In this case the highly NNSE becomes the *linear* SE, leading to a NL optical model in which the change in the NL term is proportional to a NL function of the power, $\Delta N(I)\approx-\alpha^2(P)r^2$. Although linear in ψ, the model still describes a highly NL phenomenon of solitons through the dependence of the coefficient α on the beam power P [12]. For this reason the model is referred to as the *highly nonlocal nonlinear* SE. It has been used in [14], for example, to explain the experimental observation of optical spatial solitons in nematic liquid crystals.

In the highly NLO limit, the wave equation governing the beam propagation in 3D NN media is reduced to

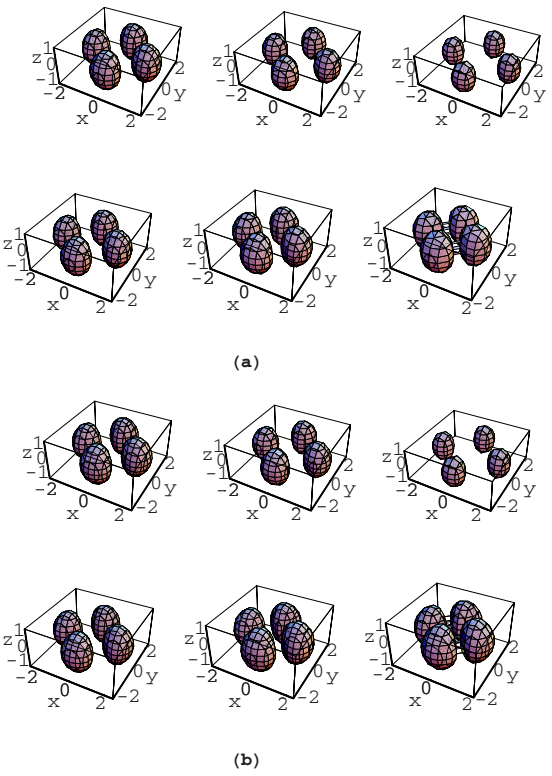

FIG. 1. (Color online) Comparison of analytical solutions with the numerical simulations for the ψ_{022} wave packet, for different parameters $\lambda=1.6$ (top row) and 0.6 (bottom row). (a) Analytical solution for intensity from Eq. (20). (b) Numerical simulation of Eq. (2). The propagation times are $2\sqrt{s}w_0^2t=0,\pi/4,\pi/2$, from left to right.

$$i\frac{\partial\psi}{\partial t}+\frac{1}{2}\nabla^2\psi-sr^2\psi=0, \tag{4}$$

where s is the parameter proportional to $\alpha^2(P)$, containing the influence of the beam power. Note that P is constant, equal to the total input power P_0. The beam intensity does not explicitly enter the evolution equation any longer, and the model becomes linear. Hence, in solving Eq. (4) we will also be solving a linear quantum mechanical problem, namely, the 3D quantum harmonic oscillator (QHO). Although many different solutions to the *time-independent* QHO in different coordinate systems are known [26], we could not locate any analytical solutions to the *time-dependent* 3D QHO. Hence, we will be looking for self-similar time-dependent solutions of Eq. (4) in the form of localized 3D wave packets. Such solutions will naturally impose certain conditions on the input parameters and the parameters describing these solutions. It should also be noted that beam collapse cannot occur in Eq. (4).

B. Self-similar solution method

The second term in Eq. (4) represents the diffraction and the third term originates from the optical nonlinearity. We treat Eq. (4) in spherical coordinates, by the method of separation of variables. Note that $s>0$. The separation of vari-

ables $\psi(t,r,\varphi,\theta)=F(t,r)Y(\varphi,\theta)$ leads to the following two equations:

$$-\frac{1}{Y}\left[\frac{1}{\sin\theta}\frac{\partial}{\partial\theta}\left(\sin\theta\frac{\partial Y}{\partial\theta}\right)+\frac{1}{\sin^2\theta}\frac{\partial^2 Y}{\partial\varphi^2}\right]=l(l+1), \quad (5)$$

$$\frac{2r^2}{F}\left[i\frac{\partial F}{\partial t}+\frac{1}{2r^2}\frac{\partial}{\partial r}\left(r^2\frac{\partial F}{\partial r}\right)-sr^2F\right]=l(l+1), \quad (6)$$

where l is a non-negative integer. Equation (5), of course, has spherical harmonics for the solution,

$$Y_{lm}(\theta,\varphi)=\sqrt{\frac{(l+m)!}{m(1+q^2)(l-m)!}}\times[\cos(m\varphi)+iq\sin(m\varphi)]P_l^m(\cos\theta), \quad (7)$$

where the parameter $q\in[0,1]$ determines the modulation depth of the beam intensity [5], and m is a real number.

Following Refs. [18,27], we define the complex field as $F(t,r)=A(t,r)e^{iB(t,r)}$, where A and B are real functions of t and r. Substituting $F(t,r)$ into Eq. (4), we find the following coupled equations for the phase $B(t,r)$ and the amplitude $A(t,r)$:

$$-A\frac{\partial B}{\partial t}+\frac{1}{r}\frac{\partial A}{\partial r}+\frac{1}{2}\frac{\partial^2 A}{\partial r^2}-\frac{1}{2}A\left(\frac{\partial B}{\partial r}\right)^2-sr^2A-\frac{l(l+1)}{2r^2}A=0, \quad (8)$$

$$\frac{\partial A}{\partial t}+\frac{\partial A}{\partial r}\frac{\partial B}{\partial r}+\frac{1}{r}A\frac{\partial B}{\partial r}+\frac{1}{2}A\frac{\partial^2 B}{\partial r^2}=0. \quad (9)$$

To find a self-similar solution of Eqs. (8) and (9), we assume that the amplitude and the phase have the forms [18,19]

$$A=\frac{k}{\sqrt{w^3}}f(\Omega), \quad (10)$$

$$B=a(t)+b(t)r+c(t)r^2, \quad (11)$$

where k is the normalization constant, $w(t)$ is the beamwidth, $f(\Omega)$ is a real function to be determined, $\Omega(t,\vec{r})$ is a self-similar variable, $a(t)$ is the phase offset, and $c(t)$ is the chirp. The functions $\Omega(t,\vec{r})$, $b(t)$, and $c(t)$, defined by the form of A and B, are found from Eq. (9): $\Omega=r/w$, $b=0$, $c=(1/2w)\partial w/\partial t$. The amplitude $A(t,r)$ is found from Eq. (8), by solving the following differential equation for f:

$$\frac{d^2f}{d\Omega^2}+\frac{2}{\Omega}\frac{df}{d\Omega}+\left[-\Omega^2\left(w^3\frac{d^2w}{dt^2}+2sw^4\right)-\frac{l(l+1)}{\Omega^2}-2w^2\frac{da}{dt}\right]f=0. \quad (12)$$

Inserting a variable transformation $f(\Omega)=\Omega^l e^{1/2-\Omega^2/2}g(\Omega)$, from Eq. (12) we obtain

$$\frac{d^2g}{d\Omega^2}+\frac{2}{\Omega}(l+1-\Omega^2)\frac{dg}{d\Omega}+\left[-\Omega^2\left(w^3\frac{d^2w}{dt^2}+2sw^4-1\right)-(2l+3)-2w^2\frac{da}{dt}\right]g=0. \quad (13)$$

To further simplify Eq. (13), we introduce another variable transformation $\Omega^2=\omega$, and after some algebra arrive at

$$\frac{d^2g}{d\omega^2}+\left(l+\frac{3}{2}-\omega\right)\frac{dg}{d\omega}+ng=0, \quad (14)$$

$$\frac{d^2w}{dt^2}+2sw-\frac{1}{w^3}=0, \quad (15)$$

$$\frac{1}{4}\left(-(2l+3)-2w^2\frac{da}{dt}\right)=n, \quad (16)$$

where n $(=0,1,2,\ldots)$ is a non-negative integer. Equation (14) is the well-known Kummer's equation, whose solutions are known as Kummer's hypergeometric functions [28], namely, $g={}_1F_1(-n,l+\frac{3}{2},\omega)$.

Taking $w(t)|_{t=0}=w_0$ and $[dw(t)/dt]|_{t=0}=0$ and integrating Eq. (15) yields [18]

$$w^2=w_0^2[1+(\lambda-1)\sin^2(2\sqrt{s}w_0^2t)], \quad (17)$$

where $\lambda=1/2sw_0^4$. Hence, from Eq. (16) and from the definition of $c(t)$, we obtain

$$a(t)=a_0-\left(2n+l+\frac{3}{2}\right)\frac{\tan^{-1}[\sqrt{\lambda}\tan(2\sqrt{s}w_0^2t)]}{2\sqrt{s}\lambda w_0^4}, \quad (18)$$

$$c(t)=\frac{\sqrt{s}w_0^2(\lambda-1)\sin(4\sqrt{s}w_0^2t)}{1+\lambda-(\lambda-1)\cos(4\sqrt{s}w_0^2t)}. \quad (19)$$

Using Eqs. (10) and (11), we finally get the exact self-similar breather solution of Eq. (4):

$$\psi_{nlm}=\frac{k[\cos(m\varphi)+iq\sin(m\varphi)]}{\sqrt{w^3}}P_l^m(\cos\theta)\left(\frac{r}{w}\right)^l\times e^{1/2-r^2/2w^2}\,{}_1F_1\left(-n,l+\frac{3}{2},\frac{r^2}{w^2}\right)e^{i[a(t)+c(t)r^2]}, \quad (20)$$

where $w(t)$, $a(t)$, and $c(t)$ are determined by Eqs. (17)–(19) and

$$k=\sqrt{\frac{2^{l+2-n}(2l+2n+1)!!}{\sqrt{\pi}n![(2l+1)!!]^2}}\sqrt{\frac{(l+m)!}{m(1+q^2)(l-m)!}}.$$

Hence, when $\lambda=1$ the beam diffraction is exactly balanced by the nonlinearity. Since $w(t)=w_0$ for $\lambda=1$, the beam width is independent of the propagation distance. The parameters are given by $w(t)=w_0$, $c(t)=0$, and $a(t)=a_0-(2n+l+\frac{3}{2})t/w_0^2$. Thus, the exact self-similar soliton solution of Eq. (4) can be written as

$$\psi_{nlm}^{s} = \frac{k[\cos(m\varphi) + iq\sin(m\varphi)]}{w_0^{3/2}} P_l^m(\cos\theta)\left(\frac{r}{w_0}\right)^l \times e^{1/2 - r^2/2w_0^2}\, {}_1F_1\left(-n, l+\frac{3}{2}, \frac{r^2}{w_0^2}\right) \times e^{i[a_0 - (2n+l+3/2)t/w_0^2]}. \quad (21)$$

III. COMPARISON WITH THE NUMERICAL SIMULATION OF THE NNSE

The breather solutions of Eq. (20) and the soliton solutions of Eq. (21) are the stable exact solutions of the linear Eq. (4). They do not represent the soliton solutions of NNSE (2), and they do not provide any hard evidence about the existence and stability of such solutions. However, there are indications of the existence and stability of similar soliton solutions coming from our numerical treatment of Eq. (2), for certain nonlocal nonlinearities.

We want to ascertain that, if one takes a breather solution as the initial field in Eq. (2) and propagates it, no instabilities develop for long propagation times. To simulate the propagation, we use the following input beam parameters:

$$\psi_{022}(0,r,\theta,\varphi) = \frac{k[\cos(2\varphi) + iq\sin(2\varphi)]}{\sqrt{w_0^3}} P_2^2(\cos\theta) \times \left(\frac{r}{w_0}\right)^2 e^{1/2 - r^2/2w_0^2}\left(1 - \frac{2r^2}{7w_0^2}\right) e^{ia_0}, \quad (22)$$

and assume that the material response is the Gaussian function (3). We also choose $\sigma_0 = 100$, so that we are in the highly NLO regime. We present contour plots above a cutoff intensity of the optical field distributions $|u_{nlm}|^2$ in 3D, choosing the initial width to be $w_0 = 1$. Figure 1 compares the analytical breather solution of Eq. (20) for $q=0$ with the numerical simulation of Eq. (2), for different λ. The numerical solution of Eq. (2) is thus performed to provide evidence on the stability of breathers in the highly NN region, and to compare with the analytical solutions. As expected, no collapse is seen, and a very good agreement with the analytical solution is obtained. Similar behavior is seen for other initial fields.

It is seen in Fig. 1 that the wave packet changes from two pairs of ellipsoids at the initial time into four smaller ellipsoids at $2\sqrt{s}w_0^2 t = \pi/2$, when $\lambda > 1$. Also, the interval between the packets in the pair expands as the beam propagates. On the contrary, the interval contracts when $\lambda < 1$, and the size of the packets increases with the propagation. The wave periodically repeats this contraction-expansion cycle, and the interval between the packets oscillates periodically as the wave propagates. Even though the solutions are presented for only one cycle of the breather evolution, the behavior persists for many cycles. For $\lambda \neq 1$, we call these wave packets the Kummer breathers.

IV. DISCUSSION OF SOLUTIONS

A. Vortex solitons

When $m=0$, from Eq. (21) one obtains Gaussian solitons. In Fig. 2 a collection of intensity distributions of Gaussian solitons with different n and l is presented. They do not change in time. For $l=0$ the soliton forms a sphere. Obviously, when all of the three parameters are zero, the soliton is called the fundamental Gaussian soliton in the 3D space. The larger n, the smaller the sphere's radius. For $l=1$, there are two layers along the vertical (z-axis) direction, and the soliton forms a pair of ellipsoids. The larger n, the flatter the ellipsoids. For $n=1$, $l>1$, the soliton forms several torus-shaped structures in the middle, but at the outside there is still a pair of ellipsoids. In general, there exist $l-1$ tori and $n+1$ pairs of ellipsoids at the outside. The maximum optical intensity is reached at the farthermost ellipsoids, along the vertical direction.

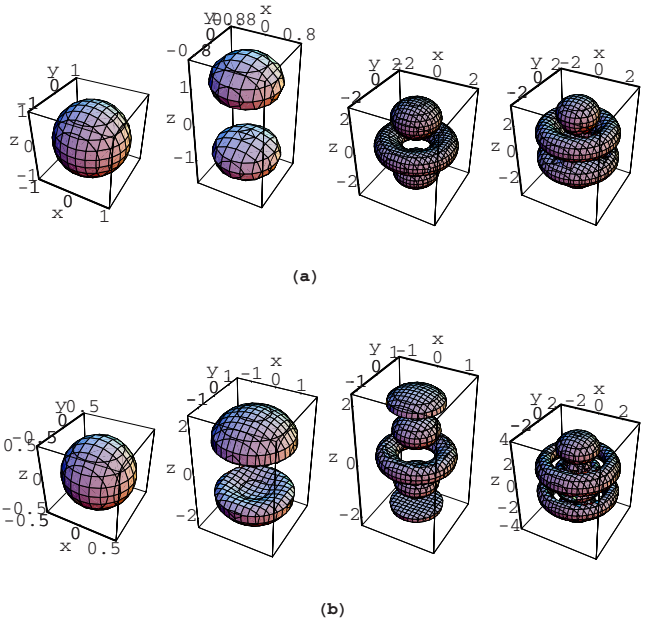

FIG. 2. (Color online) Gaussian solitons, for $m=0$. The parameters are (a) $n=0$, $l=0,1,2,3$ from left to right; (b) $n=1$, $l=0,1,2,3$ from left to right.

For $q=1$ and $m \neq 0$, one obtains vortex solitons. Figure 3(a) shows the intensity of solitons above a cutoff, with the same l,m ($l=m$) but different n. It is seen that for fixed n, the larger the parameters l and m, the flatter the soliton along the vertical direction. For different n, but still the same l and m, the larger the parameter n, the flatter the soliton along the vertical direction and also the larger the radius. The optical intensity is zero at the central point $(x,y,z)=(0,0,0)$. Figure 3(b) shows solitons with the same n, but l different from m. For equal l and n, the larger the parameter m, the smaller the soliton radius in the horizontal plane. The larger the parameter n, the flatter the soliton along the vertical direction and the larger the radius. There are $(l+1-m)$ layers along the vertical direction. The optical intensity is zero at the central point.

As seen in Fig. 3, the vortex soliton displays radial symmetry; the soliton distribution does not depend on the azimuthal angle. The physical origin of this phenomenon can qualitatively be understood from the nature of nonlocality. The NL nonlocality here means that the NL polarization of the medium has the symmetry of the electric field. Owing to the additional assumption of strong nonlocality, resulting in a

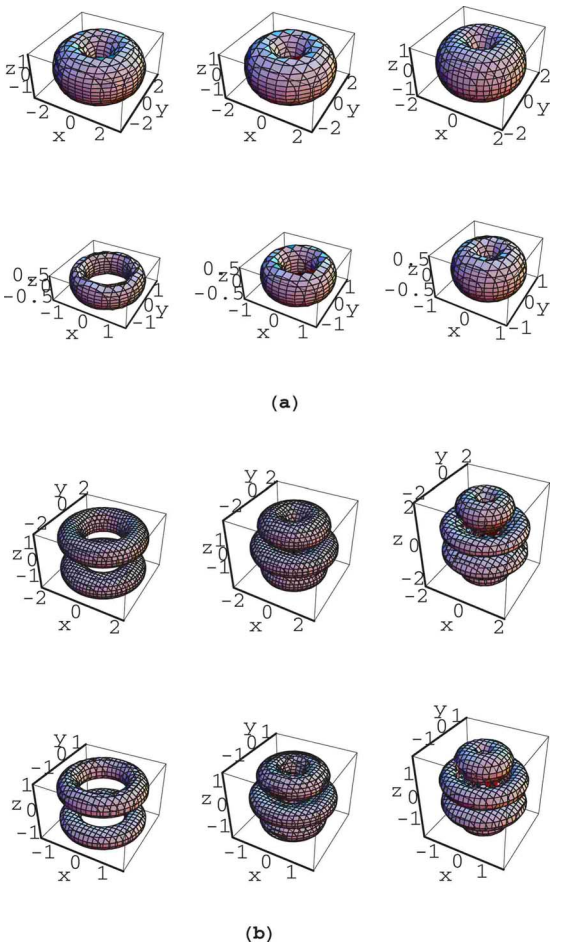

FIG. 3. (Color online) Vortex solitons, for $q=1$. (a) $l=m$; the parameters are $l=m=3,2,1$ from left to right. Top row $n=1$; bottom row $n=2$. (b) $l\neq m$, $l=4$, $m=3,2,1$ from left to right. Top row $n=1$; bottom row $n=2$.

harmonic potential, the distributions of the optical field and the intensity are obviously independent of the azimuthal angle.

B. Necklace solitons

In the limit $q=0$ and $m\neq 0$, and for some specific values of the parameters (n,m,l), we observe necklace (also called multipole) solitons. In Fig. 4 we present some examples of necklace soliton intensity. We find that the larger the parameter l, the larger the soliton radius in the horizontal plane. It is seen that the distributions change regularly with the azimuthal angle. For the same n but for different l, there are $(l+1-m)$ layers along the vertical direction. For $l=m$ solitons, the number of ellipsoids is determined by m. These multipole solitons have $2m$ ellipsoids. For $l\neq m$ ($l\neq 0$ and $m\neq 0$) solitons, the number of ellipsoids is determined by both l and m. We find that the number of ellipsoids in each layer is decided by m, and the layer number is decided by n. The necklace solitons have $2m(n+1)(l+1)$ ellipsoids, and form $n+1$ necklace layers surrounding the central point.

These characteristics of necklace solitons can be explained easily. In a highly NN medium, the refractive index

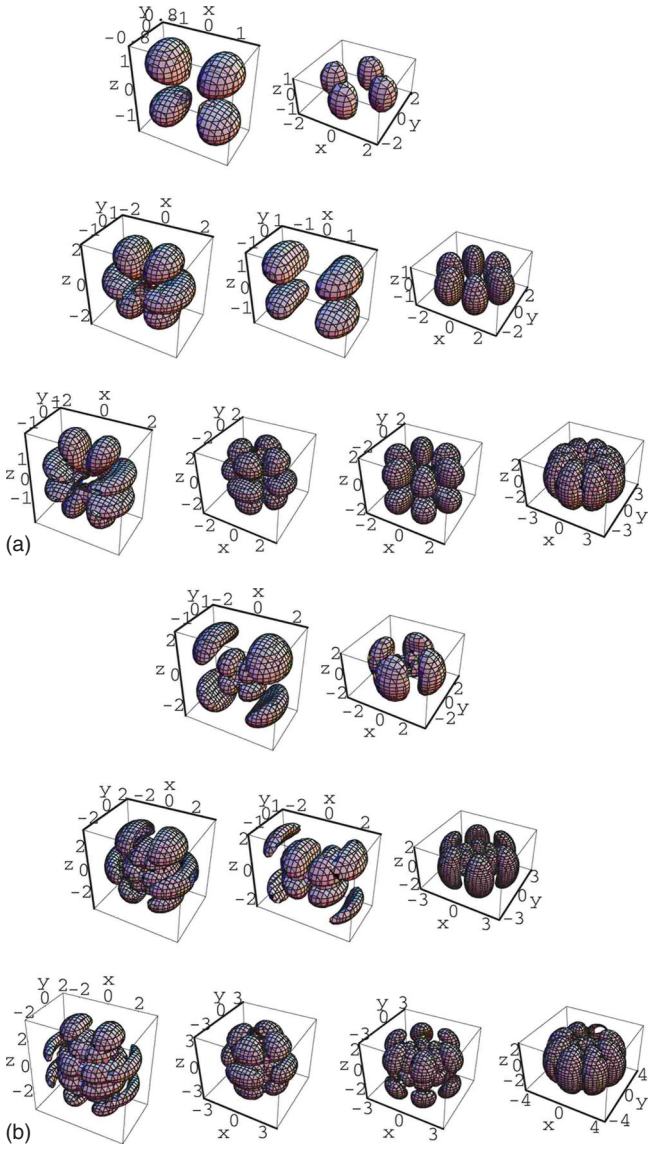

FIG. 4. (Color online) Necklace solitons. The parameters are (a) $n=0$, top row $l=2$, $m=1,2$ from left to right; middle row $l=3$, $m=1,2,3$ from left to right; bottom row $l=4$, $m=1,2,3,4$ from left to right. (b) $n=1$, top row $l=2$, $m=1,2$ from left to right; middle row $l=3$, $m=1,2,3$ from left to right; bottom row $l=4$, $m=1,2,3,4$ from left to right.

is determined by the intensity distribution over the entire transverse coordinate space, and under proper conditions the nonlocality can lead to an increase of the refractive index in the overlap region, giving rise to the formation of necklace solitons. Note that, when the NLO response function is much wider than the beam itself, the range of nonlocality in the medium is very large and the width of the refractive index distribution greatly exceeds the width of an individual light spot.

V. CONCLUSIONS

We have studied 3D self-similar spatial wave solutions of the Schrödinger equation in spherical coordinates, in the

highly NN region, both analytically and numerically. Analytical solutions have been obtained, and numerical simulations have been performed, to confirm the stability of localized solutions. The 3D self-similar spatial wave packets are built out of spherical harmonics and Kummer's hypergeometric functions. In addition to the fundamental solitons, these solutions may come in the form of 3D vortex and necklace solitons.

ACKNOWLEDGMENTS

This work was supported by the National Science Foundation of China, under Grant No. 2006CB921605, and the Science Research Foundation of Shunde College, China. The work at Texas A&M University at Qatar is supported by the NPRP 25-6-7-2 project with the Qatar National Research Foundation.

[1] Y. S. Kivshar and G. P. Agrawal, *Optical Solitons: From Fibers to Photonic Crystals* (Academic, New York, 2003).
[2] L. Paterson, M. P. MacDonald, J. Arlt, W. Sibbett, P. E. Bryant, and K. Dholakia, Science **292**, 912 (2001).
[3] T. Kuga, Y. Torii, N. Shiokawa, T. Hirano, Y. Shimizu, and H. Sasada, Phys. Rev. Lett. **78**, 4713 (1997).
[4] A. Mair, A. Vaziri, G. Weihs, and A. Zeilinger, Nature (London) **412**, 313 (2001).
[5] A. S. Desyatnikov, Y. S. Kivshar, and L. Torner, Prog. Opt. **47**, 291 (2005).
[6] M. Soljačić, S. Sears, and M. Segev, Phys. Rev. Lett. **81**, 4851 (1998).
[7] T. D. Grow, A. A. Ishaaya, L. T. Vuong, and A. L. Gaeta, Phys. Rev. Lett. **99**, 133902 (2007).
[8] A. S. Desyatnikov and Y. S. Kivshar, Phys. Rev. Lett. **87**, 033901 (2001).
[9] C. Rotschild, M. Segev, Z. Xu, Y. V. Kartashov, and L. Torner, Opt. Lett. **31**, 3312 (2006).
[10] Y. J. He, H. H. Fan, J. W. Dong, and H. Z. Wang, Phys. Rev. E **74**, 016611 (2006).
[11] Y. Cai and S. He, Opt. Express **14**, 1353 (2006).
[12] A. W. Snyder and D. J. Mitchell, Science **276**, 1538 (1997).
[13] D. Suter and T. Blasberg, Phys. Rev. A **48**, 4583 (1993).
[14] C. Conti, M. Peccianti, and G. Assanto, Phys. Rev. Lett. **92**, 113902 (2004).
[15] T. Koch, T. Lahaye, J. Metz, A. Frohlich, B. Griesmaier, and T. Pfau, Nat. Phys. **4**, 218 (2008).
[16] W. Krolikowski, O. Bang, J. J. Rasmussen, and J. Wyller, Phys. Rev. E **64**, 016612 (2001).
[17] O. Bang, W. Krolikowski, J. Wyller, and J. J. Rasmussen, Phys. Rev. E **66**, 046619 (2002).
[18] W. P. Zhong and L. Yi, Phys. Rev. A **75**, 061801(R) (2007).
[19] W. P. Zhong, M. Belić, R. H. Xie, and G. Chen, Phys. Rev. A **78**, 013826 (2008).
[20] S. Skupin, O. Bang, D. Edmundson, and W. Krolikowski, Phys. Rev. E **73**, 066603 (2006).
[21] S. Lopez-Aguayo, A. S. Desyatnikov, Y. S. Kivshar, S. Skupin, W. Krolikowski, and O. Bang, Opt. Lett. **31**, 1100 (2006).
[22] D. Buccoliero, A. S. Desyatnikov, W. Krolikowski, and Y. S. Kivshar, Opt. Lett. **33**, 198 (2008).
[23] S. Lopez-Aguayo, A. S. Desyatnikov, and Y. S. Kivshar, Opt. Express **14**, 7903 (2006).
[24] C. Rotschild, O. Cohen, O. Manela, M. Segev, and T. Carmon, Phys. Rev. Lett. **95**, 213904 (2005).
[25] M. Segev, B. Crosignani, A. Yariv, and B. Fischer, Phys. Rev. Lett. **68**, 923 (1992).
[26] R. L. Liboff, *Introductory Quantum Mechanics*, 4th ed. (Addison-Wesley, San Francisco, 2003).
[27] W. P. Zhong, L. Yi, R. H. Xie, M. Belić, and G. Chen, J. Phys. B **41**, 025402 (2008).
[28] D. Zwillinger, *Handbook of Differential Equations*, 3rd ed. (Academic, Boston, 1997).